

Classical Representation of a Quantum System at Equilibrium: Applications

Sandipan Dutta and James Dufty

Department of Physics, University of Florida

(Dated: 01 Feb 2013)

Abstract

In the preceding paper, the structure and thermodynamics of a given quantum system was represented by a corresponding classical system having an effective temperature, local chemical potential, and pair potential. Here, that formal correspondence is implemented approximately for applications to two quantum systems. The first is the electron gas (jellium) over a range of temperatures and densities. The second is an investigation of quantum effects on shell structure for charges confined by a harmonic potential.

I. INTRODUCTION

In a companion paper [1] a method was described that would allow application of strong coupling classical many body methods to calculate properties of equilibrium quantum systems. Within the grand ensemble for equilibrium statistical mechanics, the thermodynamics and structure are obtained as functions of the temperature T , the local chemical potential $\mu(\mathbf{r}) \equiv \mu - \phi_{ext}(\mathbf{r})$, and a pair potential $\phi(\mathbf{r}, \mathbf{r}')$, (where $\phi_{ext}(\mathbf{r})$ is an external single particle potential). A grand ensemble for a corresponding classical system is characterized by an effective temperature T_c , an effective local chemical potential $\mu_c(\mathbf{r}) \equiv \mu_c - \phi_{c,ext}(\mathbf{r})$, and an effective pair potential $\phi_c(\mathbf{r}, \mathbf{r}')$. These three classical parameters are fixed by three correspondence conditions: equivalence of classical and quantum pressures, densities, and pair correlation functions. An approximate inversion of these formal definitions to obtain T_c , $\mu_c(\mathbf{r})$, and $\phi_c(\mathbf{r}, \mathbf{r}')$ was described within classical liquid state theory. The objective here is to illustrate this approach for two applications. The first is to calculate the pair correlation functions for the electron gas (jellium), the prototypical test bed for quantum correlations [2, 3], over a wide range of temperatures and densities. Corresponding thermodynamic properties can then be calculated in terms of these correlation functions. The second application is to harmonically bound charges in a trap [4]. Specifically, the role of quantum diffraction and exchange as a mechanism for shell formation is investigated. While both systems have been studied extensively at both very low (ground state) and very high (plasma) temperatures, the relevance here is a method that applies across the intermediate domain.

The use of effective pair potentials to include some quantum effects in classical methods like molecular dynamics simulation has a long history [5]. A new phenomenological approach proposed by Perrot and Dharma-wardana [6] more recently goes a step farther to introduce an effective classical temperature as well. Applications of this extended approach to a variety of systems and properties over the past decade have met with remarkable success [7]. The present work can be considered as a parameter free formalization of this earlier work, and comparisons are discussed critically here as well.

In the next section, the approach of reference [1] is applied to jellium. The effective classical pair potential is discussed and illustrated, and then the pair correlation function is calculated using the classical strong coupling hypernetted chain integral equations (HNC) [8].

The dimensionless temperature relative to the Fermi temperature, $t = T/T_F$, is considered in the range $0 \leq t \leq 10$. The dimensionless measure of the density is $r_s = r_0/a_B$, the mean distance between particles defined by $4\pi r_0^3/3 = 1/n$ relative to the Bohr radius a_B . It is considered in the range $1 \leq r_s \leq 10$. The results are compared to the above mentioned model of Perrot and Dhama-wardana (PDW), and to the extension of the self-consistent generalization of the random phase approximation, STLS [9], to finite temperatures by Tanaka and Ichimaru [10]. Comparisons with limited diffusion Monte Carlo simulation data for $t = 0$ [11] and recent restricted path integral Monte Carlo simulations results for finite temperatures [12] show good agreement.

A second application is described briefly in Section III, to charges in a harmonic trap where classical strong Coulomb correlations produce shell structure [4]. These results are of interest for laser cooled ions in traps, where the quantum effects are expected to be weak, and for electrons in quantum dots at low temperatures, where the quantum effects are strong. In the classical case, strong Coulomb correlations are required for shell structure - they are absent in a mean field theory at any value of the coupling constant. The objective here is to explore possible new origins for shell structure due to quantum effects. It is shown that the quantum mean field theory, without any Coulomb correlations, leads to shell structure due to diffraction effects modifying the Coulomb interactions and/or exchange effects modifying the effective trap potential.

The results are summarized and discussed in the last section.

II. APPLICATION TO UNIFORM ELECTRON GAS

The interacting electron gas is a one component system of charges with Coulomb interactions embedded in a uniform neutralizing back ground. The uniform electron gas, or "jellium", provides an important model system to discuss correlations and quantum effects in real physical metals, solids, and plasmas [2]. The classical limit is known as the one component plasma. There are two parts to this section. First, the parameters $\beta_c = 1/k_B T_c$, $\mu_c(\mathbf{r})$, and $\phi_c(\mathbf{r}, \mathbf{r}')$ for the effective classical system are determined approximately from their definitions in reference [1] (for the uniform jellium $\mu_c(\mathbf{r}) \rightarrow \mu_c$ and $\phi_c(\mathbf{r}, \mathbf{r}') \rightarrow \phi_c(|\mathbf{r} - \mathbf{r}'|)$). Second the resulting classical system is applied to calculate the structure and thermodynamics of jellium from the classical HNC liquid state theory.

To summarize the results of [1], the classical parameters are defined as following. The classical temperature is obtained from the correspondence condition of equal pressures and the classical virial equation

$$\frac{\beta_c}{\beta} = \frac{\beta_c p_c}{\beta p} = \frac{n}{\beta p} \left[1 - \frac{n}{6} \int d\mathbf{r} h(r) \mathbf{r} \cdot \nabla \beta_c \phi_c(r) \right]. \quad (1)$$

The replacement of the pair correlation function $g(r)$ by the hole function $h(r) = g(r) - 1$ occurs because of the uniform neutralizing background. The classical activity $\beta_c \mu_c$ is given by [13]

$$\beta_c \mu_c = \ln(n_c \lambda_c^3) - n \int d\mathbf{r} \left(c(r) + \beta_c \phi_c(r) - \frac{1}{2} h(r) (h(r) - c(r)) \right), \quad (2)$$

where $c(r)$ is the direct correlation function defined in terms of $h(r)$ by the Ornstein-Zernicke equation [8]

$$c(r) = h(r) - n \int d\mathbf{r}' c(|\mathbf{r} - \mathbf{r}'|) h(r'). \quad (3)$$

Finally, the pair potential is obtained from the inversion of the HNC equation

$$\beta_c \phi_c(r) = -\ln(1 + h(r)) + h(r) - c(r). \quad (4)$$

The classical pair correlation functions on the right sides of these expressions have been replaced by the quantum functions, according to the third correspondence condition. Hence these classical parameters are determined by quantum input.

The practical approach is to provide the essential quantum input by specifying $h(r)$ in some approximation. Equations (4) and (3) then determine $\beta_c \phi_c(r)$ and $c(r)$, and with these known β_c/β and $\beta_c \mu_c$ can be calculated. The objective here is to propose a simple approximation for practical application.

1. Classical potential $\beta_c \phi_c(r)$

The dominant exchange effects are already present in the ideal gas calculation described in reference [1]. Therefore it is convenient to write $\beta_c \phi_c(r)$ in the form

$$\beta_c \phi_c(r) = (\phi_c(r))^{(0)} + \Delta(r), \quad (5)$$

where $(\phi_c(r))^{(0)}$ is the ideal gas Pauli potential and $\Delta(r)$ denotes the contribution to the effective potential from the Coulomb interactions. In the classical limit $\Delta(r) \rightarrow \beta q^2/r$.

Another exact limit is the weak coupling limit for which the direct correlation function becomes proportional to the potential, or stated inversely,

$$\beta_c \phi_c(r) \rightarrow -c(r), \quad (\beta_c \phi_c(r))^{(0)} \rightarrow -c^{(0)}(r). \quad (6)$$

Thus a possible approximation incorporating this limit is

$$\beta_c \phi_c(r) \rightarrow (\beta_c \phi_c(r))^{(0)} - (c(r) - c^{(0)}(r))^{(w)}, \quad (7)$$

where $(c(r) - c^{(0)}(r))^{(w)}$ denotes a weak coupling calculation of the direct correlation functions from the Ornstein - Zernicke equation (3). For the classical OCP (Coulomb potential) this yields the Debye - Huckel approximation to $h(r)$. Here it is required that this should yield its quantum counter part, the random phase approximation (RPA) [3]. The weak coupling calculation from the Ornstein-Zernicke equation is then

$$c(r)^{(w)} = h^{RPA}(r) - n \int d\mathbf{r}' (c(|\mathbf{r} - \mathbf{r}'|))^{(w)} h^{RPA}(r'). \quad (8)$$

This has the solution

$$c(r)^{(w)} = \frac{1}{n} \int \frac{d\mathbf{k}}{(2\pi)^3} e^{-i\mathbf{k}\cdot\mathbf{r}} \frac{S^{RPA}(k) - 1}{S^{RPA}(k)}. \quad (9)$$

Here $S^{RPA}(k)$ is the RPA static structure factor

$$S^{RPA}(k) = 1 + n \int d\mathbf{r} e^{i\mathbf{k}\cdot\mathbf{r}} h^{RPA}(r). \quad (10)$$

Finally the modified Coulomb potential $\Delta(r)$ in (5) becomes

$$\Delta(r) \rightarrow \frac{1}{n} \int \frac{d\mathbf{k}}{(2\pi)^3} e^{-i\mathbf{k}\cdot\mathbf{r}} \left(\frac{1}{S^{RPA}(k)} - \frac{1}{S^{(0)}(k)} \right). \quad (11)$$

The definition of $S^{RPA}(k)$ in terms of the RPA dielectric is given in Appendix A.

Several limits of $\Delta(r) = \Delta(t, r_s, r^*)$ are established in Appendix A. For large $r^* = r/r_0$ it behaves as r^{*-1}

$$\lim_{r^*} \Delta(t, r_s, r^*) \rightarrow \Gamma_e(t, r_s) r^{*-1}, \quad (12)$$

where $\Gamma_e(t, r_s)$ is an effective Coulomb coupling constant

$$\Gamma_e(t, r_s) = \frac{2}{\beta \hbar \omega_p \coth(\beta \hbar \omega_p / 2)} \Gamma, \quad \Gamma \equiv \frac{\beta q^2}{r_0}. \quad (13)$$

Here $\omega_p = \sqrt{4\pi n q^2 / m}$ is the plasma frequency. The dimensionless parameter is $\beta \hbar \omega_p = (4/3) (2\sqrt{3}/\pi^2)^{1/3} \sqrt{r_s}/t$ so for fixed r_s the high and low temperature limits are

$$\Gamma_e \rightarrow \begin{cases} \Gamma, & \beta \hbar \omega_p \ll 1 \\ (\frac{4}{3} r_s)^{1/2}, & \beta \hbar \omega_p \gg 1 \end{cases} \quad (14)$$

This asymptotic Coulomb form is exact and its coefficient follows from the fact that the RPA incorporates the exact perfect screening sum rule [14]. It is illustrated for $r^*\Delta(t, r_s, r^*)$ in Figure 1 at $r_s = 5$ for several values of t .

Also shown in this figure are the results from the PDW classical potential

$$(\beta_c \phi_c(r))^{PDW} = (\beta_c \phi_c(r))^{(0)} + \Delta^{PDW}(r). \quad (15)$$

The Pauli potential $(\beta_c \phi_c(r))^{(0)}$ as in is the same as in (5) but its correction $\Delta^{PDW}(r)$ is given by the Deutsch regularized Coulomb potential [15]

$$\Delta^{PDW}(r) = \beta^{PDW} \frac{q^2}{r} \left(1 - e^{-r/\lambda^{PDW}}\right), \quad \lambda^{PDW} = \left(\frac{\beta^{PDW} \hbar^2}{\pi m}\right)^{1/2}. \quad (16)$$

Here $\beta^{PDW} = 1/k_B T^{PDW}$, where $T^{PDW} \equiv (T^2 + T_0^2)^{1/2}$. The only free parameter, $T_0 = T_0(r_s)$, is fit by requiring that the classical correlation energy matches the quantum exchange/correlation energy obtained from quantum simulation at $T = 0$. The fit given in reference [6] is

$$T_0 \simeq \frac{T_F}{a + b\sqrt{r_s} + cr_s}, \quad (17)$$

with $a = 1.594$, $b = -0.3160$, and $c = 0.0240$. It is seen that the PDW model is quite similar to the approximation defined here at $r_s = 5$. Greater discrepancies occur for both larger and smaller r_s except at higher temperatures. Further comments on this comparison are given below.

For $r^* \ll 1$, $\Delta(t, r_s, r^*)$ approaches a finite value

$$\Delta(t, r_s, 0) = \frac{1}{n} \int \frac{d\mathbf{k}}{(2\pi)^3} \left(\frac{1}{S^{RPA}(k)} - \frac{1}{S^{(0)}(k)} \right). \quad (18)$$

The integral converges because the static structure factors for large k approach 1 as k^{-4} due to quantum effects (cusp condition [16]). The Coulomb singularity is therefore removed in the effective classical pair potential. Finally, another limit obtained in the Appendix A is that for large r_s and large t (low density, high temperature) in which case the Kelbg potential [17] is recovered

$$\lim_{t, r_s \gg 1} \Delta(t, r_s, r^*) \rightarrow \Delta_K(t, r^*) = \frac{\Gamma}{r^*} \left(1 - \exp\left(2\pi \frac{r_0^2}{\lambda_K^2} r^{*2}\right) + \sqrt{2\pi} \frac{r_0}{\lambda_K} r^* (1 - \operatorname{erf}(\sqrt{2\pi} \frac{r_0}{\lambda_K} r^*)) \right), \quad (19)$$

with $\lambda_k = \lambda/\sqrt{2\pi}$. The Kelbg potential is the exact weak coupling effective classical potential determined from the two particle electron - electron density matrix [17]. This limit is approached to within 10 percent at $t = 10$ and $1 \leq r_s \leq 10$.

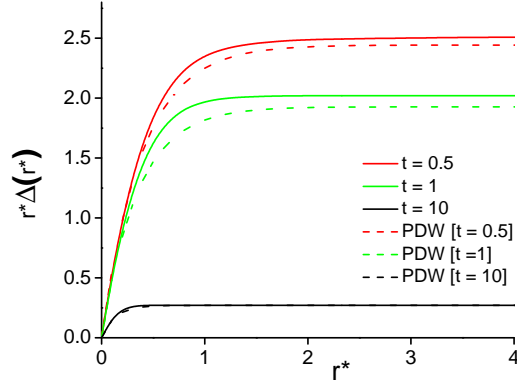


FIG. 1: (color online) Demonstration of crossover for $r^*\Delta(t, r_s, r^*)$ to Coulomb with effective coupling constant $\Gamma_e(t, r_s)$ given by eq.(13), for $r_s = 5$ and $t = 0.5, 1, 10$. Also shown are the corresponding results for $r^*\Delta_{PDW}(t, r_s, r^*)$.

2. Classical effective temperature, chemical potential

The approximate temperature and chemical potential equations are obtained in a similar way

$$\beta_c = \beta_c^{(0)} + (\beta_c^{RPA} - \beta_c^{RPA,(0)}) . \quad (20)$$

$$\beta_c \mu_c = (\beta_c \mu_c)^{(0)} + (\beta_c \mu_c)^{RPA} - (\beta_c \mu_c)^{RPA,(0)} , \quad (21)$$

where $\beta_c^{(0)}$ and $(\beta_c \mu_c)^{(0)}$ denote the ideal gas results of [1], and from (1) and (2)

$$\beta_c^{RPA} = \frac{n \left[1 - \frac{n}{6} \int d\mathbf{r} h^{RPA}(r) \mathbf{r} \cdot \nabla (\beta_c \phi_c(r))^{RPA} \right]}{p^{RPA}} , \quad (22)$$

$$(\beta_c \mu_c)^{RPA} = \frac{3}{2} \ln \left(\frac{\beta_c^{RPA}}{\beta} \right) + \ln (n \lambda^3)^{RPA} + \frac{1}{2} n \int d\mathbf{r} h^{RPA}(r) \left(h^{RPA}(r) + (\beta_c \phi_c(r))^{RPA} \right) . \quad (23)$$

The RPA results for p^{RPA} and $(n \lambda^3)^{RPA}$ are computed from the Pade fits of reference [2].

A peculiarity of jellium is the possibility for the pressure to become negative at large r_s and small t , conditions for which the equal pressures correspondence condition cannot be imposed. For real systems, the pressure is positive as follows from the convexity of the free energy as a function of the volume. This convexity does not hold for jellium [13]. To be more explicit, it is first noted that the pressure is an increasing function of t so its minimum value occurs at $t = 0$. Figure 2 shows the quantum p^{RPA} at $t = 0$ as a function on r_s . It

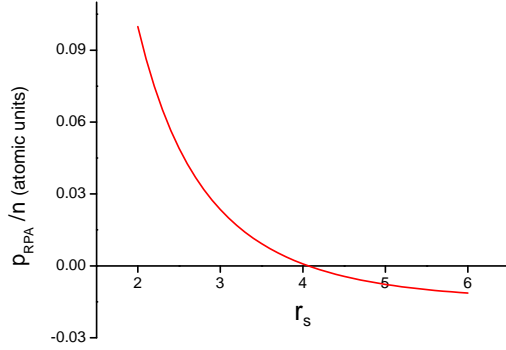


FIG. 2: (color online) Quantum RPA pressure p_{RPA} at $t = 0$ as a function of r_s .

is seen that $p^{RPA}(t = 0)$ vanishes for $r_s \simeq 4$, and becomes negative for larger r_s . Thus for $r_s \gtrsim 4$ the pressure $p^{RPA}(t)$ vanishes at some temperature $t_0(r_s)$. Then from (20) and (22), the effective classical temperature vanishes at t_0

$$T_c(t_0(r_s)) = \frac{p^{RPA}(t_0)}{n \left[1 - \frac{n}{6} \int d\mathbf{r} h^{RPA}(r) \mathbf{r} \cdot \nabla (\beta_c \phi_c(r))^{RPA} \right]} = 0. \quad (24)$$

For $t < t_0(r_s)$, $p^{RPA}(t) < 0$. However, it is found that the denominator of (24) remains positive. Since the classical temperature must be positive this indicates that the equivalence condition, $p_{cl} = p$, can no longer be realized. Therefore for jellium, this one of the equivalence conditions should be replaced by a different condition (e.g., equivalence of internal energies). Instead, the analysis here is restricted to $t > t_0(r_s)$ to assure positive pressure. Figure 3 shows $t_c = T_c/T_F$ as a function of t calculated from (20) for $r_s = 0, 1, 3, 4$, and 5. Figure 4 shows the corresponding results for μ_c/E_F calculated from (21).

A. Radial distribution function and thermodynamics

With the parameters of the effective classical system determined approximately above they can be used in an accurate classical many-body method to combine the quantum properties of these parameters with classical strong coupling effects (e.g., molecular dynamics simulation). This is illustrated here by using the full HNC integral equations (4) and (3)

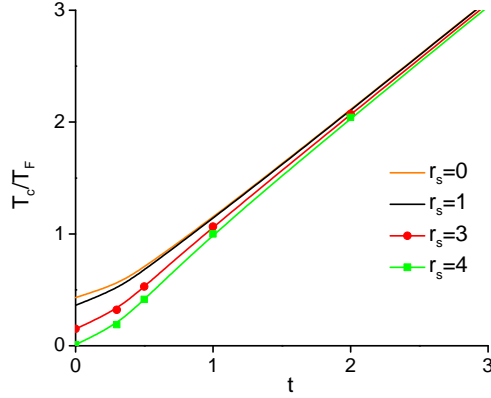


FIG. 3: (color online) Classical reduced temperature T_c/T_F as a function of t for $r_s = 0, 1, 3$ and 4.

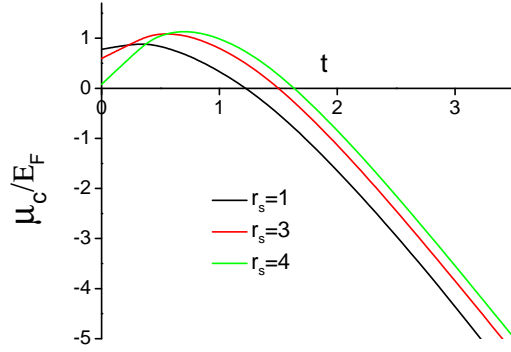


FIG. 4: (color online) Dimensionless classical chemical potential μ_c/E_F as a function of t for $r_s = 1, 3, 5$.

specialized to calculate $g(r)$ for jellium

$$\ln g(r) = -\beta_c \phi_c(r) + h(r) - c(r), \quad c(r) = h(r) - n \int d\mathbf{r}' c(|\mathbf{r} - \mathbf{r}'|) h(r'). \quad (25)$$

Of course, these equations are also those used to define $\beta_c \phi_c(r)$ so the analysis would seem to be circular. However, the approach has been to use an approximation to the HNC equations to determine $\beta_c \phi_c$ (here the weak coupling RPA limit) and then to "bootstrap" this information to solve the full HNC equations for a $g(r)$ that goes beyond the input $g^{RPA}(r)$ to include classical strong coupling. One manifest improvement obtained in this

way is positivity of $g(r)$, already noted in [6]. In contrast, $g^{RPA}(r)$ becomes negative for small r at sufficiently large r_s .

The determination of $g(r)$ from (25) is straightforward using the method described in reference [18]. Note that these equations do not use the equal pressure condition nor the value of β_c . Hence they do not have the restriction to positive pressures and the associated restriction on r_s . The results are shown in Figure 5 for the case of $r_s = 6$ at $t = 0.5, 1, 4$ and 8. Also shown are the results from recent restricted PIMC [12]. The agreement is quite good. Figure 6 shows the same conditions as Figure 5 for comparison with the classical map of PDW. The agreement is remarkable given that the forms and origins of the effective classical parameters is so different. This agreement between the predictions here, PIMC, and PDW extends to other state conditions as well, except for small t and very large r_s .

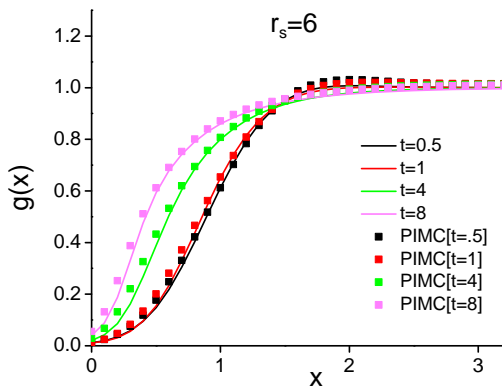


FIG. 5: (color online) Radial distribution function $g(r^*)$ for $r_s = 6$ at $t = 0.5, 1, 4, 8$. Also shown are the results of PIMC.

Other theoretical models for $g(r)$ are based on the same dielectric formalism of the RPA, but including "local field" corrections. One of the earliest was the self-consistent STLS model [9] at $T = 0$, later generalized to finite temperature T by Tanaka and Ichimaru (TI) [10]. The discrepancies (not shown) are largest at lower t and most noticeably at small distances where TI becomes negative. The RPA results are significantly more negative in this range. Both RPA and its improved TI overestimate the size of the electron correlation hole [3] at larger values for r_s .

The PDW $g(r)$ is in good agreement with diffusion MC data at $t = 0$ [6] for $r_s = 1, 5, 10$. Although the single parameter T_0 is fixed by fitting the $t = 0$ exchange/correlation energy

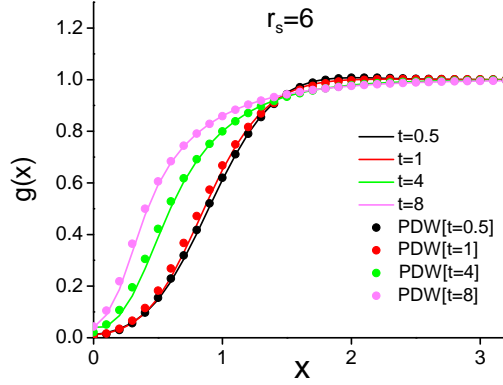


FIG. 6: (color online) Radial distribution function $g(r^*)$ for $r_s = 6$ at $t = 0.5, 1, 4, 8$. Also shown are the results of PDW.

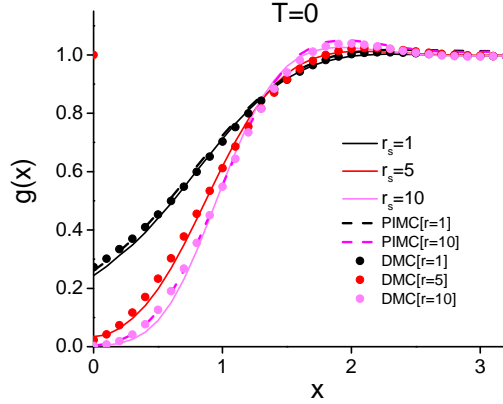


FIG. 7: Radial distribution function $g(r^*)$ for $t = 0$ at $r_s = 1, 5, 10$. Also shown are results from PIMC and diffusion Monte Carlo. The PIMC and diffusion Monte Carlo plots are indistinguishable.

from MC data it is nevertheless impressive that this provides good results for $g(r)$ across a range both r_s and r . Figure 7 shows a comparison of the results of the present analysis with the same $T = 0$ diffusion MC data [11], and also the recent PIMC for $T = 0.065$ at $r_s = 1, 10$. The good agreement is quite surprising since there is no MC parametrization in the present analysis and all quantum input is via the RPA and ideal gas exchange. However, it is recalled that the RPA preserves the exact quantum mechanics of the perfect screening sum rule that governs the cross over to exact large r^* Coulomb limit. This is discussed further in the last section.

1. Thermodynamics

The predicted pressure, p_c in atomic units, for the effective classical system is obtained from

$$\frac{\beta_c p_c}{n_c} = 1 - \frac{1}{6} n \int d\mathbf{r} h(r) \mathbf{r} \cdot \nabla \beta_c \phi_c(r). \quad (26)$$

and the effective temperature (22). Figure 8 shows this as a function of t for $r_s = 1, 3, 4$ and 5. Also shown are the corresponding results for modified RPA (using the fits from reference [19]).

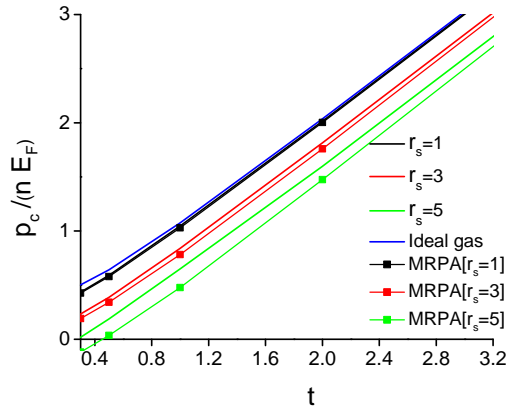


FIG. 8: (color online) Dimensionless classical pressure $p_c/(nE_F)$ as a function of t for $r_s = 1, 3, 5$. Also shown are the corresponding modified RPA results.

III. APPLICATION TO CHARGES IN A HARMONIC TRAP

As a final application here consider \bar{N} charges localized within a harmonic trap. The Hamiltonian is

$$H - \mu N = \sum_{i=1}^N \frac{p_i^2}{2m} + \frac{1}{2} \sum_{i \neq j}^N \frac{q^2}{|\mathbf{r}_i - \mathbf{r}_j|} - \int d\mathbf{r} \mu(\mathbf{r}) \hat{n}(\mathbf{r}), \quad (27)$$

with the local chemical potential given explicitly as

$$\mu(\mathbf{r}) = \mu - \frac{1}{2} m \omega^2 r^2. \quad (28)$$

The constant μ determines the average number of charges \bar{N} . As a consequence of the harmonic potential the equilibrium average density profile for the charges is non-uniform

and depends only on the radial coordinate

$$n(r) = \Omega^{-1} \sum_{N=0}^{\infty} N \int d\mathbf{r}_2 \dots d\mathbf{r}_N \langle \mathbf{r}_1 \dots \mathbf{r}_N | e^{-\beta(H-\mu N)} | \mathbf{r}_1 \dots \mathbf{r}_N \rangle, \quad (29)$$

where $\langle \mathbf{r}_1 \dots \mathbf{r}_N | X | \mathbf{r}_1 \dots \mathbf{r}_N \rangle$ is the N particle diagonal anti-symmetric matrix element in coordinate representation, and Ω is the grand potential. The density profile in the classical limit has been studied in detail, via simulation and theory [4]. In that case the dimensionless form depends on r_s and t only through the Coulomb coupling constant $\Gamma = \beta q^2 / r_0 = (4/3) (2/3\pi^2)^{1/3} r_s / t$. For sufficiently large Γ the formation of shell structure is observed in $n(r)$. The objective now is to exploit this effective classical description to explore the effects of quantum diffraction and exchange via the proposed effective classical system. Only a preliminary investigation of new mechanisms for shell structure is described here, with a more complete discussion to be given elsewhere.

The basis for the study is the HNC description for the inhomogeneous case, Eq. (37) of reference [1]

$$\ln(n(\mathbf{r}) \lambda_c^3) = \beta_c \mu_c(\mathbf{r}) + \int d\mathbf{r}' c^{(2)}(\mathbf{r}, \mathbf{r}' | n) n(\mathbf{r}'). \quad (30)$$

The classical studies of reference [4] made a further approximation to this expression, replacing the correlations for the inhomogeneous system $c^{(2)}(\mathbf{r}, \mathbf{r}'' | n)$ by those for a corresponding uniform one component plasmas (OCP or classical jellium), $c^{(2)}(\mathbf{r}, \mathbf{r}'' | n) \rightarrow c(|\mathbf{r} - \mathbf{r}''|, n)$. The results based on this approximation are found to be quite accurate except at very strong coupling. A partial theoretical basis has been given [20]. This approximation will be made here as well.

It is convenient to rewrite (30) in a Boltzmann form with an effective potential $U(\mathbf{r})$ defined by

$$n(\mathbf{r}) = \bar{N} \frac{e^{-\beta_c U(\mathbf{r})}}{\int d\mathbf{r}' e^{-\beta_c U(\mathbf{r}')}}, \quad (31)$$

so that (30) becomes

$$\beta_c U(\mathbf{r}) = -\beta_c (\mu_c(\mathbf{r}) - \mu_c) - \frac{\bar{N}}{\int d\mathbf{r}' e^{-\beta_c U(\mathbf{r}')}} \int d\mathbf{r}' e^{-\beta_c U(\mathbf{r}')} c(|\mathbf{r} - \mathbf{r}'|, n). \quad (32)$$

Practical application of this result requires specification of the direct correlation function $c(r, n)$ for jellium and the classical local chemical potential $\mu_c(\mathbf{r}) - \mu_c$. The former is determined from the equivalent classical calculation described in the previous section. The latter

is the effective classical trap potential corresponding to the actual quantum harmonic trap. It's approximate determination is described in the next subsection.

The total number of particles appears explicitly. To introduce the density, it is necessary to assign a volume for the system. This can be defined as the volume of a sphere with radius R_0 corresponding to a particle at the greatest distance from the center. At equilibrium the average density can be taken to be spherically symmetric so that the total average force on that particle is

$$\frac{\bar{N}q^2}{R_0^2} - m\omega^2 R_0 = 0, \quad \Rightarrow R_0^3 = \bar{N} \frac{q^2}{m\omega^2}. \quad (33)$$

This gives the average density to be

$$\bar{n} \equiv \frac{3\bar{N}}{4\pi R_0^3} = \frac{3m\omega^2}{4\pi q^2}. \quad (34)$$

In this way, the trap parameter $m\omega^2/q^2$ is specified in terms of the density.

A. Approximate form for $\mu_c(\mathbf{r})$

Without quantum effects $\mu_c - \mu_c(\mathbf{r})$ is just the harmonic potential of (28). Modifications for the effective classical form occur due to both diffraction and exchange effects. The exchange effects are dominated by those for the ideal Fermi gas in a harmonic trap. As a first approximation here, $\mu_c(\mathbf{r})$ is replaced by that for an ideal gas of \bar{N} Fermions in a harmonic trap. This is the inhomogeneous ideal gas considered in Section IV in [1]. The local chemical potential is therefore obtained from (30) specialized to an ideal gas

$$(\beta_c \mu_c)^{(0)}(\mathbf{r}) = \ln(n^{(0)}(\mathbf{r})\lambda_c^3) - \int d\mathbf{r}' c^{(0)}(|\mathbf{r} - \mathbf{r}'|) n^{(0)}(\mathbf{r}'). \quad (35)$$

Then the effective potential $U(\mathbf{r})$ becomes

$$\beta_c U(\mathbf{r}) = -\ln(n^{(0)}(\mathbf{r})\lambda_c^3) - \int d\mathbf{r}' c^{(0)}(|\mathbf{r} - \mathbf{r}'|) n^{(0)}(\mathbf{r}') + \beta_c \mu_c - \bar{N} \int d\mathbf{r}' \frac{e^{-\beta_c U(\mathbf{r}')}}{\int d\mathbf{r}'' e^{-\beta_c U(\mathbf{r}'')}} c(|\mathbf{r} - \mathbf{r}'|, n). \quad (36)$$

The direct correlation function for the uniform ideal Fermi gas, $c^{(0)}(r, n)$, is known from the results of [1]. Furthermore, $n^{(0)}(\mathbf{r})$ has an explicit form in the local density approximation of Appendix B, reference [1]

$$n^{(0)}(\mathbf{r}) = \frac{2}{\lambda^3} f_{3/2} \left(e^{(\beta\mu^{(0)} - \frac{1}{2}\Gamma r^{*2})} \right). \quad (37)$$

where Γ is the same coupling constant as in eqn (13). The Fermi function $f_{3/2}(x)$ is given by

$$f_{3/2}(z) = \frac{4}{\sqrt{\pi}} \int_0^\infty dx x^2 \left(z^{-1} e^{x^2} + 1 \right)^{-1}. \quad (38)$$

The constant chemical potential $\mu^{(0)}$ is determined in terms of t, r_s by the condition that the average number of particles is \bar{N}

$$\bar{N} = 2 \left(\frac{r_0}{\lambda} \right)^3 \int d\mathbf{r}^* f_{3/2} \left(e^{\beta(\mu^{(0)} - \frac{1}{2}\Gamma r^{*2})} \right). \quad (39)$$

Hence $n^{(0)}(\mathbf{r})r_0^3$ is also given by (37) in terms of t, r_s . Figure 9 shows $\beta_c \phi_{c,ext}(\mathbf{r}) \equiv (\beta_c \mu_c)^{(0)}(\mathbf{r}) - (\beta_c \mu_c)^{(0)}(\mathbf{0})$ obtained in this way for $r_s = 5$ and $t = 0.5, 1, 5$, and 10. The classical trap potential is harmonic at large r , but there are significant deviations at the lower temperatures for $2 \lesssim r \lesssim 3$.

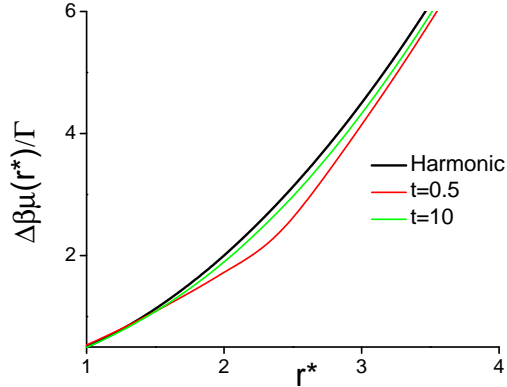


FIG. 9: (color online) Effective classical trap potential $\Delta\beta_c\mu_c(\mathbf{r}^*)/\Gamma = (\beta_c\mu_c(\mathbf{r}^*) - \beta_c\mu_c(\mathbf{0}))/\Gamma$ as a function of r^* for $t = 0.5, 10$. Also shown is the harmonic potential.

B. Quantum effects on the mean field density profile

The density profile can now be determined from (32) where the effective potential of (35) becomes

$$\beta_c U(\mathbf{r}) = \beta_c \phi_{c,ext}(\mathbf{r}) - \bar{N} \int d\mathbf{r}' \frac{e^{-\beta_c U(\mathbf{r}')}}{\int d\mathbf{r}'' e^{-\beta_c U(\mathbf{r}'')}} c(|\mathbf{r} - \mathbf{r}'|, n). \quad (40)$$

(the potential $\beta_c U(\mathbf{r})$ has been shifted by a constant to simplify the result). The effective classical external trap potential is

$$\beta_c \phi_{c,ext}(\mathbf{r}) = -\ln(n^{(0)}(\mathbf{r})\lambda^3) + \int d\mathbf{r}' c^{(0)}(|\mathbf{r} - \mathbf{r}'|) n^{(0)}(\mathbf{r}') \quad (41)$$

Quantum effects result from the deviation of $\beta_c \phi_{c,ext}(\mathbf{r})$ from the given harmonic potential, and the deviation of $c(r, n)$ from its classical OCP form. In this section these two sources are isolated to explore the possibility of new origins of shell structure. To do so only the mean field limits of (40) and (41) are explored here. The mean field limit is defined by $c(r, n) \rightarrow -\beta_c \phi_c(r)$ and $c^{(0)}(r, n) \rightarrow -(\beta_c \phi_c(r))^{(0)}$ so (40) and (41) become

$$\beta_c U(\mathbf{r}) \rightarrow \beta_c \phi_{c,ext}(\mathbf{r}) + \bar{N} \int d\mathbf{r}' \frac{e^{-\beta_c U(\mathbf{r}')}}{\int d\mathbf{r}'' e^{-\beta_c U(\mathbf{r}'')}} \left[(\beta_c \phi_c(|\mathbf{r} - \mathbf{r}'|))^{(0)} + \Delta(|\mathbf{r} - \mathbf{r}'|) \right], \quad (42)$$

$$\beta_c \phi_{c,ext}(\mathbf{r}) \rightarrow -\ln(n^{(0)}(\mathbf{r})\lambda^3) - \int d\mathbf{r}' (\beta_c \phi_c(|\mathbf{r} - \mathbf{r}'|))^{(0)} n^{(0)}(\mathbf{r}'). \quad (43)$$

The classical mean free limit corresponds to $(\beta_c \phi_c(r))^{(0)} = 0$ and $\Delta(r) = \beta q^2/r$. There is no shell structure in this limit, even at very strong coupling. Instead, shell structure arises due to sufficiently large Coulomb coupling, such that $c(r, n)$ differs from $-\beta q^2/r$ inside the correlation length r_0 and the Coulomb singularity at $r = 0$ is removed. This is shown in Figure 10 for $\Gamma = 3$.

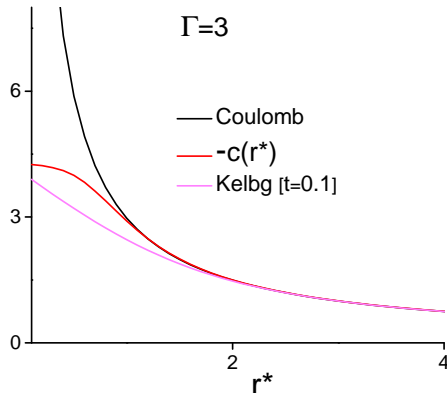


FIG. 10: (color online) Comparison of $-c(r^*)$ and $V_K(r^*)$ at $t = 0.1, 0.27$ both corresponding to $\Gamma = 3$. Also shown is the Coulomb limit $\beta q^2/r$.

1. Diffraction effects

To explore the effects of diffraction only in (42) and (43), the contributions from exchange are set to zero, i.e. $(\beta_c \phi_c(r))^{(0)} \rightarrow 0$, $\beta_c \phi_{c,ext}(\mathbf{r}) \rightarrow m\omega^2 r^2/2$, and $\Delta(r) \rightarrow \Delta_K(r) = \text{Kelbg}$, eq. (19). Then (42) becomes

$$\beta_c U(\mathbf{r}) \rightarrow \beta_c \frac{1}{2} m\omega^2 r^2 + \bar{N} \int d\mathbf{r}' \frac{e^{-\beta_c U(\mathbf{r}')}}{\int d\mathbf{r}'' e^{-\beta_c U(\mathbf{r}'')}} \beta \Delta_K(|\mathbf{r} - \mathbf{r}'|), \quad (44)$$

This has the same form as the classical limit, except with the Coulomb potential replaced by the Kelbg form. The latter differs from Coulomb at short distances, for which it is finite at $r = 0$. Thus diffraction (without Coulomb correlations) leads to the same qualitative physical effects as classical Coulomb correlations. This is illustrated in Figure 10 where the Kelbg potential is evaluated at $r_s = 0.042$, $t = 0.1$ and at $r_s = 0.11$, $t = 0.27$ both corresponding to $\Gamma = 3$. For this reason it can be expected that the quantum diffraction mean field approximation can give rise to shell structure not present in the corresponding classical case. This is shown in Figure 11 for $\Gamma = 3$ and $t = 0.1, 0.5, 1, 2$. A clear shell formation occurs at the two lowest temperatures, for which the diffraction regularization of $\Delta_K(\mathbf{0})$ is greatest.

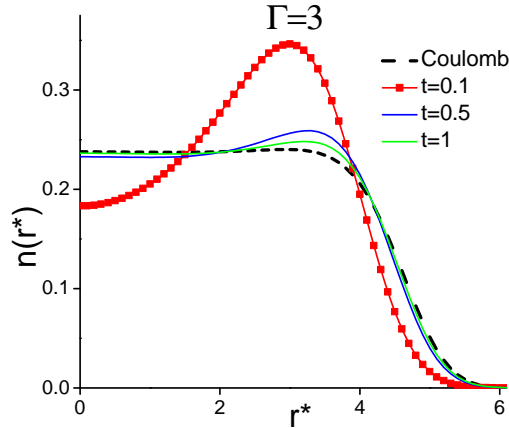


FIG. 11: (color online) Diffraction mean field approximate density profile for $\Gamma = 3$ and $t = 0.1, 0.5, 1$.

2. Exchange effects

Now return to the mean field form (42) and neglect all diffraction effects to study the effects of exchange only

$$\beta_c U(\mathbf{r}) \rightarrow \beta_c \phi_{c,ext}(\mathbf{r}) + \bar{N} \int d\mathbf{r}' \frac{e^{-\beta_c U(\mathbf{r}')}}{\int d\mathbf{r}' e^{-\beta_c U(\mathbf{r}')}} \left[(\beta_c \phi_c(|\mathbf{r} - \mathbf{r}'|))^{(0)} + \beta q^2 |\mathbf{r} - \mathbf{r}'|^{-1} \right], \quad (45)$$

This differs from the classical form by the addition of the exchange Pauli potential to the Coulomb potential, and by the modifications of the harmonic trap form in $\phi_{c,ext}(\mathbf{r})$, Figure 9. If the latter are neglected it is expected that no shell structure will appear, since the Pauli plus Coulomb potential is still singular at short range and behaves as the classical mean field limit. The quantitative changes in $\phi_{c,ext}(\mathbf{r})$ shown in Figure 9 are modest for $t \geq 2$, but there is a qualitative change in shape for $2 < r^* < 3$ at lower temperatures. The corresponding density profiles from (45) are shown in Figure 12 at $r_s = 5$. Shell formation in this range is clearly seen for $t = 1$ and 0.5.

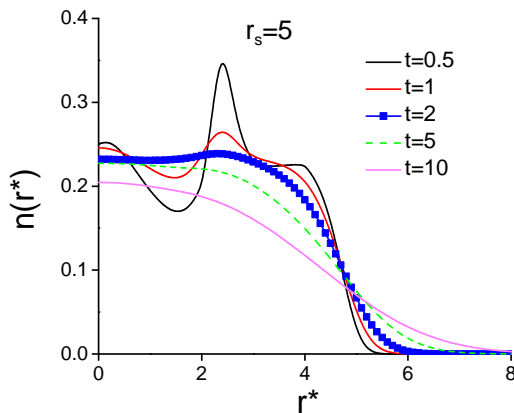


FIG. 12: (color online) Exchange mean field approximate density profile for $r_s = 5$ and $t = 0.5, 1, 2, 5, 10$.

IV. DISCUSSION

There are powerful many body methods within classical equilibrium statistical mechanics that do not apply directly to quantum systems. Examples are molecular dynamics simulation and liquid state theory. To bridge this gap a method to define an equivalent classical

system for the thermodynamics and structure of a given quantum system has been developed [1]. The objective here has been to demonstrate and test that approach with applications to two quite different quantum systems, the bulk uniform electron gas and charges confined by a harmonic trap. In the first case, a simple representation for the pair potential incorporating both ideal gas exchange and RPA correlations was used within a strong coupling classical theory - the HNC. Essential properties such as positivity are assured by the classical formalism, in contrast to early quantum theories with mean field corrections to RPA. Good agreement with diffusion Monte Carlo simulation over a range of densities at $t = 0$. Initial comparisons with recent results at finite t [12] also show good agreement. A more extensive comparison will be discussed elsewhere.

The good agreement at $t = 0$ is more than might be expected from the RPA input for the classical pair potential. The PDW model also has similar agreement but is parameterized by exchange correlation simulation data at $t = 0$ so agreement is less surprising. One possible explanation for the results here is the preservation of the exact perfect screening sum rule. This assures that the effective potential in the approximation used here has the exact Coulomb tail for large r , (12) and (13). Elsewhere, a simple analytic model is constructed which incorporates this asymptotic property. Its comparison with Monte Carlo simulation data for $g(r)$ has accuracy comparable to that of the results presented here.

The second application here was to charges confined by a harmonic trap. This is an interesting test system for strong correlations since classically this is reflected in the formation of radial shell structure. Here, only the mean field theory (no Coulomb correlations) was considered as a means to explore the possibility of purely quantum mechanisms for shell structure. It was found that diffraction effects, which regularize the Coulomb potential at $r = 0$ mimic classical Coulomb correlations and does lead to shell structure. In addition, in the absence of both diffraction effects and Coulomb correlations, the changes in the effective confining potential due to exchange effects also can lead to shell structure. Elsewhere, a detailed application of this effective classical system will be described with all mechanisms for shell structure active.

V. ACKNOWLEDGEMENTS

This research has been supported by NSF/DOE Partnership in Basic Plasma Science and Engineering award DE-FG02-07ER54946 and by US DOE Grant DE-SC0002139.

Appendix A: RPA for the Uniform Electron Gas

In this Appendix the RPA is defined and it is shown that the modified Coulomb potential reduces to the Kelbg potential for weak coupling and weak degeneracy. More generally, the exact large r dependence of this potential is evaluated.

The static structure factor is related to the Fourier transform of the hole function by

$$S(k) = 1 + n \int d\mathbf{r} e^{i\mathbf{k}\cdot\mathbf{r}} h(r). \quad (\text{A1})$$

As a density fluctuation it is also related to the dynamic response function or complex dielectric function $\epsilon(\omega, k)$ [3]:

$$S(k) = -\frac{\hbar}{\pi} \frac{1}{\tilde{V}(k)} \int_{-\infty}^{\infty} d\omega (1 - e^{-\beta\hbar\omega})^{-1} \text{Im} \epsilon^{-1}(k, \omega), \quad (\text{A2})$$

where $\tilde{V}(k) = 4\pi q^2/k^2$ is the Fourier transformed Coulomb potential. In the random phase approximation the dielectric function is

$$\epsilon^{RPA}(k, \omega) = 1 - \tilde{V}(k) \chi^{(0)}(\omega, k), \quad (\text{A3})$$

and $\chi^{(0)}(\mathbf{k}, \omega)$ is the response function for the ideal Fermi gas

$$\chi^{(0)}(\mathbf{k}, \omega) \equiv \frac{(2s+1)}{n} \lim_{\eta \rightarrow 0^+} \int \frac{d\mathbf{k}_1}{(2\pi)^3} \frac{n(\epsilon_{|\mathbf{k}-\mathbf{k}_1|}) - n(\epsilon_{k_1})}{\hbar\omega + i\eta + e_{k_1} - e_{|\mathbf{k}-\mathbf{k}_1|}}, \quad e_k = \frac{\hbar^2 k^2}{2m} \quad (\text{A4})$$

1. Kelbg limit

For weak coupling $\epsilon^{-1}(k, \omega)$ can be expanded to quadratic order in $\tilde{V}(k)$ to get

$$S(k) \rightarrow S^{(0)}(k) - 2\frac{\hbar}{\pi} \tilde{V}(k) \int_{-\infty}^{\infty} d\omega (1 - e^{-\beta\hbar\omega})^{-1} (\text{Im} \chi^{(0)}(\omega, k)) (\text{Re} \chi^{(0)}(\omega, k)). \quad (\text{A5})$$

The real and imaginary parts of $\chi^{(0)}(\omega, k)$ are

$$\text{Re} \chi^{(0)}(\mathbf{k}, \omega) = -\frac{(2s+1)}{n\lambda^3} \beta \frac{1}{4\sqrt{\pi\kappa}} \mathcal{P} \int_{-\infty}^{\infty} dx \ln(1 + ze^{-x^2}) \left(\frac{1}{\nu + \kappa - x} - \frac{1}{\nu - \kappa - x} \right) \quad (\text{A6})$$

$$\text{Im } \chi^{(0)}(\mathbf{k}, \omega) = \frac{(2s+1)}{n\lambda^3} \beta \frac{\sqrt{\pi}}{4\kappa} \ln \left(\frac{1 + ze^{-(\nu+\kappa)^2}}{1 + ze^{-(\nu-\kappa)^2}} \right). \quad (\text{A7})$$

The dimensionless variables κ and ν are

$$\kappa = \frac{k\lambda}{4\sqrt{\pi}}, \quad \nu = \frac{\beta\hbar\omega}{4\kappa}, \quad \lambda = \left(\frac{2\pi\beta\hbar^2}{m} \right)^{1/2}. \quad (\text{A8})$$

Next consider the additional limit of weak degeneracy. This is implemented by an expansion in z

$$S^{(0)}(k) \rightarrow 1 + \mathcal{O}(z), \quad n\lambda^3 \rightarrow (2s+1)z, \quad (\text{A9})$$

$$\text{Re } \chi^{(0)}(\mathbf{k}, \omega) \rightarrow \frac{\beta}{4\kappa} (g(\nu+\kappa) - g(\nu-\kappa)) \quad (\text{A10})$$

$$\text{Im } \chi^{(0)}(\mathbf{k}, \omega) \rightarrow \beta \frac{\sqrt{\pi}}{4\kappa} \left(e^{-(\nu+\kappa)^2} - e^{-(\nu-\kappa)^2} \right). \quad (\text{A11})$$

with

$$g(y) = -\frac{1}{\sqrt{\pi}} \mathcal{P} \int_{-\infty}^{\infty} dx e^{-x^2} \frac{1}{y-x} = -2e^{-\nu^2} \int_0^{\nu} dx e^{x^2}. \quad (\text{A12})$$

The RPA structure factor becomes

$$\begin{aligned} S(k) &\rightarrow 1 + \beta \tilde{V}(k) \frac{1}{2\kappa\sqrt{\pi}} \int_{-\infty}^{\infty} d\nu e^{-(\nu-\kappa)^2} (g(\nu+\kappa) - g(\nu-\kappa)) \\ &= 1 + \beta \tilde{V}(k) \frac{1}{2\kappa\sqrt{2}} g(\sqrt{2}\kappa) \end{aligned} \quad (\text{A13})$$

The modified Coulomb potential at weak coupling and weak degeneracy becomes

$$\begin{aligned} \Delta(r) &= \frac{1}{n} \int \frac{d\mathbf{k}}{(2\pi)^3} e^{-i\mathbf{k}\cdot\mathbf{r}} \left(\frac{1}{S^{RPA}(k)} - \frac{1}{S^{(0)}(k)} \right) \\ &\rightarrow -\frac{1}{n} \int \frac{d\mathbf{k}}{(2\pi)^3} e^{-i\mathbf{k}\cdot\mathbf{r}} \beta \tilde{V}(k) \frac{1}{2\kappa\sqrt{2}} g(\sqrt{2}\kappa) \\ &= \beta V_K(r) \end{aligned} \quad (\text{A14})$$

This is the Kelbg potential of eq. (19).

2. Large r limit

The large r behavior of $\Delta(r)$ is governed by the small k behavior of $S^{RPA}(k)$

$$S^{RPA}(k) \rightarrow \frac{\hbar k^2}{2m\omega_p} \coth\left(\frac{\beta\hbar\omega_p}{2}\right). \quad (\text{A15})$$

This is the exact perfect screening behavior [14] which is preserved by the RPA. Since $S^{(0)}(0)$ is finite at finite t and vanishes as k for $t = 0$,

$$\begin{aligned}\Delta(r) &= \frac{1}{n} \int \frac{d\mathbf{k}}{(2\pi)^3} e^{-i\mathbf{k}\cdot\mathbf{r}} \left(\frac{1}{S^{RPA}(k)} - \frac{1}{S^{(0)}(k)} \right) \\ &\rightarrow \frac{m\omega_p}{2\pi n\hbar \coth(\frac{\beta\hbar\omega_p}{2})} \int \frac{d\mathbf{k}}{(2\pi)^3} e^{-i\mathbf{k}\cdot\mathbf{r}} \frac{4\pi}{k^2} \\ &= \Gamma_e(t, r_s) r^{*-1}, \quad \Gamma_e(t, r_s) \equiv \frac{2}{\beta\hbar\omega_p \coth(\frac{\beta\hbar\omega_p}{2})} \Gamma,\end{aligned}\tag{A16}$$

where $\Gamma = \beta q^2/r_0$ is the classical Coulomb coupling constant. This is the result of eq. (13).

-
- [1] J. Dufty and S. Dutta, *Classical Representation of a Quantum System at Equilibrium: Theory*, previous paper in this journal.
- [2] D. Kremp, M. Schlanges, W. Kraeft, *Quantum Statistics of Nonideal Plasmas*, (Springer-Verlag, Berlin, 2005).
- [3] G. Giuliani and G. Vignale, *Quantum Theory of the Electron Liquid*, (Cambridge U. Press, Cambridge, 2005)
- [4] J. Wrighton, J. W. Dufty, H. Kählert, and M. Bonitz, Phys. Rev. E **80**, 066405 (2009).
- [5] C. Jones and M. Murillo, High Energy Density Physics **3**, 379 (2007); F. Graziani et al, High Energy Density Physics **8**,105 (2012).
- [6] M. W. C. Dharma-wardana and F. Perrot, Phys. Rev. Lett. **84**, 959 (2000); F. Perrot and M. W. C. Dharma-wardana, Phys. Rev. B **62**, 16536 (2000).
- [7] M. W. C. Dharma-wardana, Int. J. Quant. Chem. 112, **53** (2012).
- [8] J-P Hansen and I. MacDonald, *Theory of Simple Liquids*, (Academic Press, San Diego, CA, 1990).
- [9] K. Singwi, A. Sjolander, M. Tosi, and R. Land, Phys. Rev. **B1**, 1044 (1970).
- [10] S. Tanaka and S. Ichimaru, J. Phys. Soc. Japan **55**, 2278 (1986).
- [11] G. Ortiz and P. Ballone, Phys. Rev. B **50**, 1391 (1994).
- [12] E. Brown, B. Clark, J. DuBois, D. Ceperley, *Path Integral Monte Carlo Simulation of the Warm-Dense Homogeneous Electron Gas*, cond mat arXiv:1211.6130, 2012.
- [13] M. Baus and J.P. Hansen, Phys. Rep. **59** (1980) 1; M. Baus, Physica **79A**, 377 (1975).

- [14] D. Pines and Ph. Nozieres, *The Theory of Quantum Liquids*, (Benjamin, NY, 1966); D. Brydges and Ph. Martin, *J. Stat. Phys.* **96**, 1163 (1999).
- [15] C. Deutsch, *Phys. Lett. A* **60**, 317 (1977); H. Minoo, M. Gombert, and C. Deutsch, *Phys. Rev. A* **23**, 924 (1981).
- [16] J. Kimball, *Phys. Rev. A* **7**, 1648 (1973); A. Rajagopal, J. Kimball, and M. Banerjee, *Phys. Rev. B* **18**, 2339 (1978).
- [17] G. Kelbg, *Ann. Phys.* **12**, 219 (1963); A. Filinov, V. Golubnychiy, M. Bonitz, W. Ebeling, and J. Dufty, *Phys. Rev. E* **70**, 046411 (2004).
- [18] K-C Ng, *J. Chem. Phys.* **61**, 2680 (1974).
- [19] F. Perrot and M. W. C. Dharma-wardana, *Phys. Rev. A* **30**, 2169 (1984).
- [20] J. Wrighton, H. Kählert, T. Ott, P. Ludwig, H. Thomsen, J. Dufty, and M. Bonitz, *Contrib. Plasma Phys.* **52**, 45 (2012); arXiv: 1110.2465.